

RESEARCH

Open Access



LC-MS/MS based metabolomics reveals the mechanism of skeletal muscle regeneration

Lei Yi¹, Kaiming Wang^{1†}, Sui Liufu¹, Wenwu Chen¹, Bohe Chen¹, Xiaolin Liu¹, Caihong Liu¹, Jingwen Liu¹, Xin Xu¹ and Haiming Ma^{1,2,3*}

Abstract

Background Skeletal muscle possesses a robust regenerative capacity and can effectively repair itself following injury. However, research on the metabolic changes during skeletal muscle regeneration in large animals remains relatively limited. Therefore, in this study, we used pigs as a model and applied non-targeted LC-MS/MS metabolomic technology to reveal the metabolic changes during skeletal muscle regeneration, and conducted an in-depth exploration of important signaling pathways, which can provide a reference for further research on the mechanisms promoting skeletal muscle regeneration.

Methods In this study, we used 18 piglets aged 35 days and weighing 7.10 ± 0.90 kg to construct a skeletal muscle regeneration model. These piglets were randomly divided into three treatment groups ($n=6$) and injected with cardiotoxins (CTX) in the right longissimus dorsi muscle. They were euthanized on the 1st, 4th, and 16th days post-injection to collect right longissimus dorsi muscle samples as the treatment group. Additionally, the left longissimus dorsi muscle of piglets on the 4th day post-injection was selected as the control group. Phenotypic changes in skeletal muscle regeneration were determined through H&E staining, immunofluorescence, and Western Blot analysis, and LC-MS/MS untargeted metabolomics technology was utilized to explore the differential expressed metabolites (DEMs) involved in skeletal muscle regeneration.

Results Phenotyping results showed that the regeneration model showed 3 stages of inflammation, regeneration and remodeling, which indicated successful model construction. Non-targeted LC-MS/MS metabolomics analysis showed significant differences in the structure of metabolites in these 3 stages. (1) In the inflammatory stage, a total of 198 DEMs were identified, which were mainly enriched in the pathways regulating the inflammatory response. (2) in the repair stage, 264 DEMs were identified, which were mainly enriched in pathways that inhibit inflammatory response and promote protein synthesis. (3) During the remodeling stage, 102 DEMs were identified, which were mainly enriched in the pathways that inhibit protein depletion and promote protein deposition. Temporal expression analysis revealed metabolites consistent with changes in the skeletal muscle regeneration process and found that these metabolite functions were mainly enriched in inhibiting inflammatory responses, alleviating myofibrillar lysis,

[†]Kaiming Wang contributed equally to this work and should be considered co-first author.

*Correspondence:
Haiming Ma
mahaiming2000@163.com

Full list of author information is available at the end of the article



and promoting muscle growth. Among them, (R)-Lipoic acid, 8-Hydroxyguanosine, and Uridine 5'-monophosphate maybe key metabolites associated with skeletal muscle regeneration.

Conclusion The skeletal muscle regeneration mechanism was systematically explored, and the metabolite time series analysis during skeletal muscle regeneration revealed some key metabolites that reflect the degree of skeletal muscle damage.

Keywords Skeletal muscle regeneration, LC-MS/MS, Metabolomics

Background

The muscles that are located in the trunk and limbs, attached to bones, are known as skeletal muscles, constituting approximately 40% of the adult human body. Mechanical or pathological injuries to skeletal muscles are common in human activities and animal husbandry. Such injuries may lead to muscle fiber necrosis and changes in muscle mass, resulting in impaired muscle function [1]. Skeletal muscle has a robust regenerative capacity after injury, which is coordinated by a network of interactions among various cell types [2, 3]. In the event of skeletal muscle injury, muscle regeneration occurs in three overlapping stages: inflammation, repair, and remodeling. During the inflammatory stage, damaged cells release signaling molecules that activate the clotting and complement cascades, leading to neutrophil infiltration, macrophage activation, and satellite cell activation [4]. During the repair stage, macrophages remove necrotic tissue debris, MuSCs are activated and give rise to myoblasts, which further proliferate, differentiate, and fuse to form multinucleated myotubes [1, 5]. During the remodeling stage, damaged muscle fibers fuse with myogenic cells to repair the fibers or generate new muscle fibers to replace the necrotic fibers, thus restoring the structure and function of the skeletal muscle [6]. The proliferation and differentiation of MuSCs is called muscle regeneration, which is not only important for the growth and development of skeletal muscle, but also plays a crucial role in skeletal muscle regeneration.

Although many studies have attempted to reveal the complex process of muscle regeneration, the precise mechanisms of skeletal muscle regeneration are still not clear. In addition to serving as a locomotor organ, skeletal muscle also acts as an endocrine organ, capable of secreting a variety of factors to regulate muscle repair and regeneration functions under different conditions. Research by Chi et al. has shown that macrophages promote the formation of liquid-liquid phase separation condensates of fibroblast growth factor (FGF) on the cell membrane surface by releasing 11,12-epoxyeicosatrienoic acid (11,12-EET), significantly increasing the binding efficiency of FGF to its receptor FGFR, thereby further activating the downstream PI3K-Akt-mTOR and MAPK signaling pathways, and promoting the proliferation and differentiation of MuSCs [7]. In addition, Psat1

regulates the biosynthetic pathway of serine by producing α -ketoglutarate (α -KG) and glutamine in MuSCs, which affects the proliferation and differentiation of MuSCs and myogenic progenitor cells, and plays an important regulatory role in the regeneration of mouse skeletal muscle [8]. Another study found that the chemokine CXCL7 released by platelets plays a key role in muscle regeneration by guiding the recruitment of neutrophils and regulating inflammatory responses [9]. These findings highlight the importance of metabolic changes in skeletal muscle regeneration and reveal a close connection between metabolic changes and muscle repair and regeneration.

Therefore, delving deeply into the metabolic changes during skeletal muscle regeneration is crucial for elucidating its molecular mechanisms. Metabolomics can effectively capture subtle alterations in the body's biological processes, bridging the gap between genetics and phenotype, and fully reflecting the complex interplay of genetic and environmental factors [10]. However, there is limited research on metabolomics studies of skeletal muscle regeneration. Studies have shown that pigs and humans share high similarities in anatomical size and structure, physiology, immunology, and genomics, making pigs an important biomedical model for studying human diseases [11, 12]. Cardiotoxin (CTX) is a commonly used drug to induce skeletal muscle necrosis, trigger acute inflammatory responses in skeletal muscle, and stimulate the repair and remodeling of skeletal muscle [13]. In the current construction of skeletal muscle regeneration models, there is no unified standard for the selection of time points. In Song et al.'s study, CTX was injected into the tibialis anterior muscle of mice, and the post-injection time points of Day 3, Day 7, and Day 14 were chosen as the 3 stages of skeletal muscle regeneration [1]. In Ma et al.'s study, bupivacaine hydrochloride was injected into the longissimus dorsi muscle of pigs, with time points of 0 h, 2 h, Day 1, Day 3, Day 5, and Day 7 chosen to study the stages of skeletal muscle regeneration [14]. Here, we chose pigs as the model and injected CTX to induce muscle injuries, triggering skeletal muscle inflammation and promoting skeletal muscle regeneration [15]. Referring to the time point selection in the above-mentioned skeletal muscle regeneration models, we chose Day 1, Day 4, and Day 16 after CTX injection

in pigs as the inflammatory response stage, repair stage, and remodeling stage of skeletal muscle regeneration, respectively. Through metabolomics analysis, we investigated the changes in metabolites during skeletal muscle regeneration and systematically explored the mechanisms involved in the process. Our research findings provide new insights into the relationship between skeletal muscle metabolic changes and the process of skeletal muscle regeneration, revealing key metabolites with practical value in promoting skeletal muscle regeneration and maintaining normal development.

Methods

Animal samples

All animal experiments in this study were approved by the Institutional Animal Care and Use Committee of Hunan Agricultural University, Changsha, Hunan Province, China, with approval number CACAHU 20230701. In this study, eighteen piglets aged 35 days with a weight of 7.10 ± 0.90 kg were randomly divided into 3 treatment groups, with $n=6$ in each group, consisting of 3 males and 3 females. The right longissimus dorsi muscle was injected with 1 mL of 40 μ M CTX (9012-91-3, BOYAO, Shanghai, China) to establish a skeletal muscle injury repair model. The left longissimus dorsi muscle (non-injected side) of the piglets euthanized on the 4th day was chosen as the control group. The pigs were euthanized on the 1st, 4th, and 16th days after injection. Samples of the longissimus dorsi muscle were taken from the injection site and the non-injected side, immediately frozen in liquid nitrogen, and stored at -80 °C for subsequent experiments.

Paraffin sectioning and Hematoxylin-Eosin staining (H&E)

Fresh muscle tissues were fixed in 4% paraformaldehyde for 24 h, then dehydrated with ethanol and xylene. After paraffin embedding, sections were cut to a thickness of 5 μ m. The sections were sequentially placed in Xylene I for 20 min, Xylene II for 20 min, anhydrous ethanol I for 5 min, anhydrous ethanol II for 5 min, and 75% alcohol for 5 min, then washed with water. The sections were stained with hematoxylin for 3–5 min, differentiated, and blued. Stained with eosin for 5 min, and finally sealed with neutral gum. The cross-sectional area (CSA) of the myofibers was quantitatively assessed using the Image-Pro Plus 6.0 software (Media Cybernetics). This analysis involved 3 fields from each view and 6 different views for each sample.

Immunofluorescence

After fixing the fresh muscle tissue, the tissue is sequentially treated with xylene I, xylene II, anhydrous ethanol I, anhydrous ethanol II, 85% alcohol, and 75% alcohol, and finally washed with distilled water to dewax the paraffin

sections to water. Then, using EDTA antigen retrieval buffer, the sections are treated in a microwave for antigen retrieval. The tissue is circled using an immunohistochemical pen and blocked with 3% hydrogen peroxide, then blocked with serum and added with primary antibody MYH3 (AF300260, AiFang biological, China), and incubated overnight at 4 °C. Add HRP-labeled secondary antibody (AFIHC003, AiFang biological, China), then add CY3-TSA, counterstain cell nuclei with DAPI, add autofluorescence quencher, seal with anti-fluorescence quenching sealer, and finally examine and take photos under a fluorescence microscope.

Western blot

The total protein was extracted using a RIPA-lysed buffer with protease inhibitors and protein phosphatase inhibitors (Abiowell, Changsha, China). Protein concentration was determined by the BCA method. 10 μ g of protein was separated by SDS-PAGE gel electrophoresis. Subsequently, the separated proteins were transferred to a polyvinylidene fluoride (PVDF) membrane. Then, it was blocked with 5% skim milk for 2 h, and incubated with primary antibody for PCNA (ET1605-38, HUA-BIO, Suzhou, China) or PAX7 (ET1612-60, HUABIO, Suzhou, China) at 4 °C for 12 h. After washing the PVDF membrane, it was incubated with a secondary antibody (BF03008X, Biodragon, China) for 2 h. Finally, protein bands were visualized using chemiluminescent reagents and quantified using ImageJ.

Sample preparation for metabolomics analysis

A 100 mg muscle tissue sample was placed into a 2 mL centrifuge tube with a 6 mm diameter grinding bead. The metabolites were extracted using 400 μ L of a methanol: water (4:1, v/v) extraction solution containing 0.02 mg/mL internal standard (L-2-chlorophenylalanine). The sample solution was ground in a frozen tissue grinder (-10 °C, 50 Hz, 6 min), followed by low-temperature ultrasonic extraction for 30 min (5 °C, 40 kHz). Subsequently, the samples were allowed to stand at -20 °C for 30 min, followed by centrifugation (4 °C, 13000 rpm, 15 min). The supernatant was then transferred to a new vial for subsequent LC-MS/MS analysis. To ensure consistency, equal amounts of all samples were combined to create quality control (QC) samples. Throughout the analysis, one QC sample was included after every eight muscle tissue samples and subjected to the same treatment as the analysis samples to verify the reproducibility of the entire analytical process.

LC-MS/MS analysis

The LC-MS/MS analysis of the samples was performed at Majorbio Bio-Pharm Technology Co. Ltd. in Shanghai, China, using the UHPLC-Q Exactive system

equipped with an HSS T3 chromatographic column (100 mm×2.1 mm i.d., 1.8 μm). Following separation on the HSS T3 column, 2 μL of the sample entered the mass spectrometry detector. The mobile phase consisted of 95% water + 5% acetonitrile (containing 0.1% formic acid) as mobile phase A and 47.5% acetonitrile + 47.5% isopropanol + 5% water (containing 0.1% formic acid) as mobile phase B. The flow rate was set at 0.40 mL/min, and the column temperature was maintained at 40°C. Mass spectrometric signals of the samples were acquired in both positive and negative ionization modes, with a mass scanning range of *m/z* 70–1050. The ion spray voltage was 3500 V for positive ions and 2800 V for negative ions, sheath gas flow rate was 40 psi, auxiliary gas flow rate was 10 psi, ion source heating temperature was set at 400°C, collision energies were set at 20–40–60 V, MS1 resolution was 70,000, and MS2 resolution was 17,500.

Untargeted metabolomics analysis of skeletal muscle

Upon completion of the LC-MS run, the raw data were imported into the metabolomics processing software Pregenesis QI (Waters Corporation, Milford, USA) for preprocessing and exported as a 3-dimensional data matrix in CSV format. The MS and MSMS mass spectrometric information were matched with the metabolite public databases HMDB (<http://www.hmdb.ca/>) and Metlin (<https://metlin.scripps.edu/>) along with an in-house database to retrieve metabolite information. The data matrix retrieved from the databases was uploaded to the Majorbio Cloud Platform (<https://cloud.majorbio.com>) for data analysis. Initially, the data matrix was preprocessed as follows: variables with non-zero values in at least one sample group exceeding 80% were retained, and any missing values were filled in (using the smallest value in the original matrix). To minimize errors caused by sample preparation and instability, the response intensities of the sample spectral peaks were normalized using the total sum scaling method, yielding a normalized data matrix. Variables with a relative standard deviation (RSD) > 30% in the QC samples were simultaneously removed, and the data were log₁₀ transformed to obtain the final data matrix. The R package “ropls” (Version 1.6.2) was used for principal component analysis (PCA) and orthogonal partial least squares discriminant analysis (OPLS-DA), and the stability of the model was assessed using seven-fold cross-validation. Additionally, DEMs were determined based on the variable importance in projection (VIP) values obtained from the OPLS-DA model and the *p*-values from the student's *t*-test, with metabolites with VIP > 1 and *p* < 0.05 regarded as DEMs. The DEMs were annotated with metabolic pathways using the KEGG database (<https://www.kegg.jp/kegg/pathway.html>) to identify the pathways in which the metabolites participate. Pathway enrichment analysis

was performed using the Python package *scipy stats*, and the biological pathways most closely related to the experimental treatment were identified using the Fisher's exact test.

Statistical analysis

Data analysis was conducted using GraphPad Prism 8.0 for one-way analysis of variance (ANOVA). Significance was determined through independent sample *t*-tests, and two-tailed tests were used for significance testing. Results are presented as mean ± standard error of the mean (SEM), with *p* < 0.05 denoting significant differences and *p* < 0.01 indicating highly significant differences.

Results

Histological and molecular level changes during skeletal muscle regeneration after injury

Pigs are commonly used models for animal diseases. To reveal the metabolic changes during the repair process of skeletal muscle injury in large animals, CTX is used to induce damage to the right longissimus dorsi muscle, thereby triggering the regeneration process of skeletal muscle (Fig. 1A). H&E staining was used for tissue analysis. The results showed that on the 1st day, muscle fibers began to dissolve and break down, showing inflammation. On the 4th day, muscle fibers completely dissolved and regeneration occurred. On the 16th day, muscle fibers were remodeled and returned to their normal state (Figs. 1B–C). Myosin Heavy Chain 3 (MYH3) is a signature gene for skeletal muscle regeneration. Immunofluorescence staining showed that MYH3 appeared on the 1st day, peaked on the 4th day, and returned to normal levels on the 16th day (Figs. 1D–E). Proliferating Cell Nuclear Antigen (PCNA) is an important marker gene for identifying the proliferation state of muscle cells, and Paired Box 7 (Pax7) is a key transcription factor for MuSCs. Western blot analysis showed that the expression of PCNA gradually increased on the 1st and 4th days, indicating that the cells at the damaged site were in a highly active proliferative state, and returned to normal levels by Day 16. Similarly, the expression of PAX7 exhibited a similar trend, suggesting that the MuSCs at the damaged site were highly active on the 1st and 4th days, and returned to normal levels by Day 16 (Figs. 1F–H). The above results indicate that our skeletal muscle regeneration model was successfully constructed and can be used for subsequent experiments.

LC-MS/MS analysis and multivariate statistical analysis of skeletal muscle tissue

To determine the differential levels of metabolites during the process of skeletal muscle regeneration, we conducted LC-MS/MS untargeted metabolomics. After data preprocessing, when the standard deviation/mean (RSD)

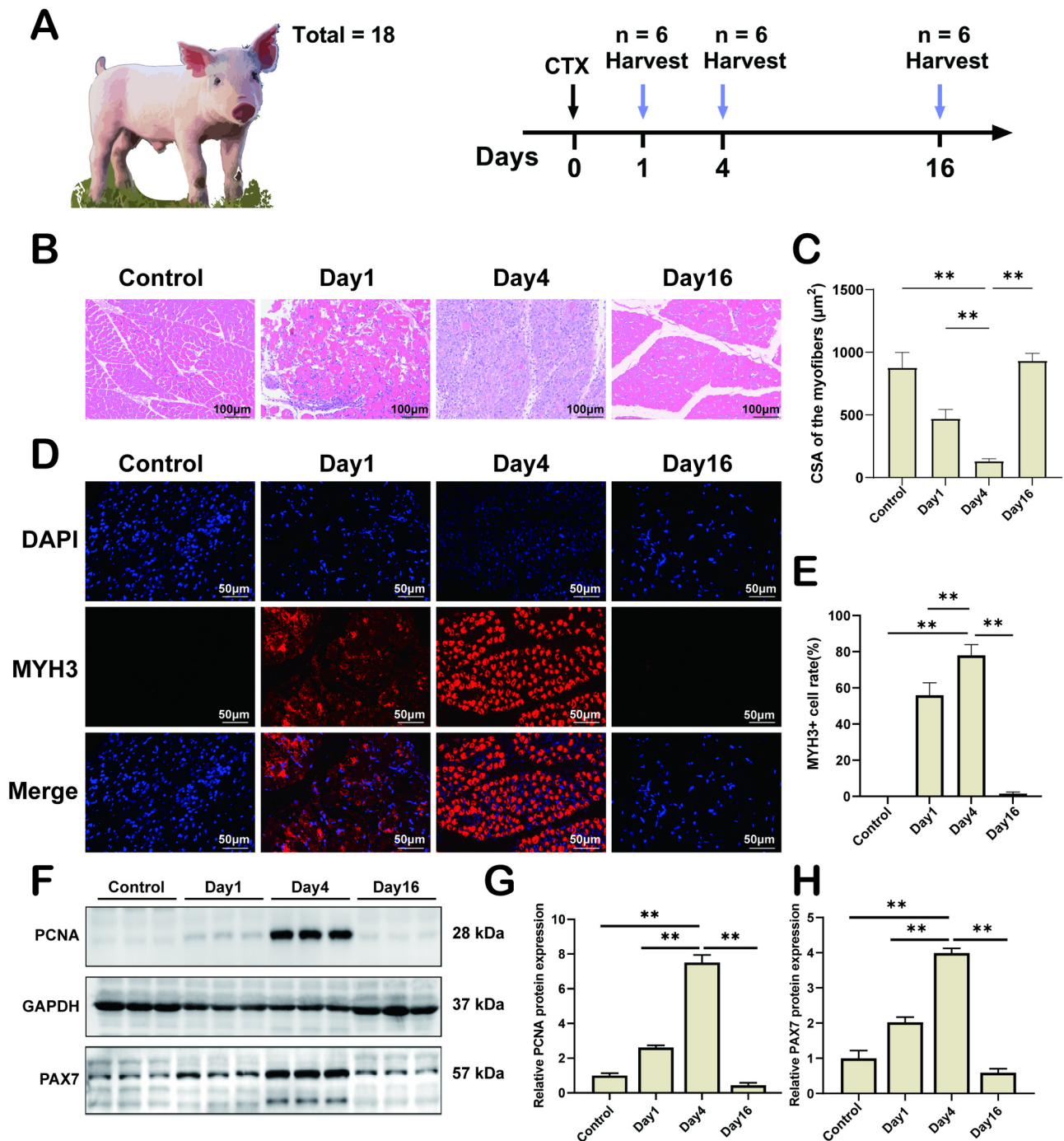


Fig. 1 CTX injection causes skeletal muscle inflammation and induces skeletal muscle regeneration. **(A)** Pig skeletal muscle regeneration model and schematic diagram. **(B)** H&E cross-sectional staining of muscle tissue at different stages of skeletal muscle regeneration (H&E, scale bar = 100 μm). **(C)** Quantification of the cross-sectional area of muscle fibers shown in B. **(D)** MYH3 immunofluorescence staining at different stages of skeletal muscle regeneration (scale bar = 100 μm). **(E)** Quantification of the percentage of MYH3⁺ cells of the total cells shown in D. **(F)** Expression level of PCNA protein in skeletal muscle tissue at different stages of regeneration. **(G)** Quantification of PCNA protein expression levels shown in F. **(H)** Quantification of PAX7 protein expression levels shown in F.

of the QC samples was <30%, the cumulative area of the peaks was >70% (Fig. 2A), so the QC samples were qualified. The collected data were then subjected to multivariate statistical analysis using the R package ropls

(Version1.6.2), including principal component analysis (PCA) and orthogonal partial least squares discriminant analysis (OPLS-DA). The effectiveness and applicability of the OPLS-DA model were validated by permutation

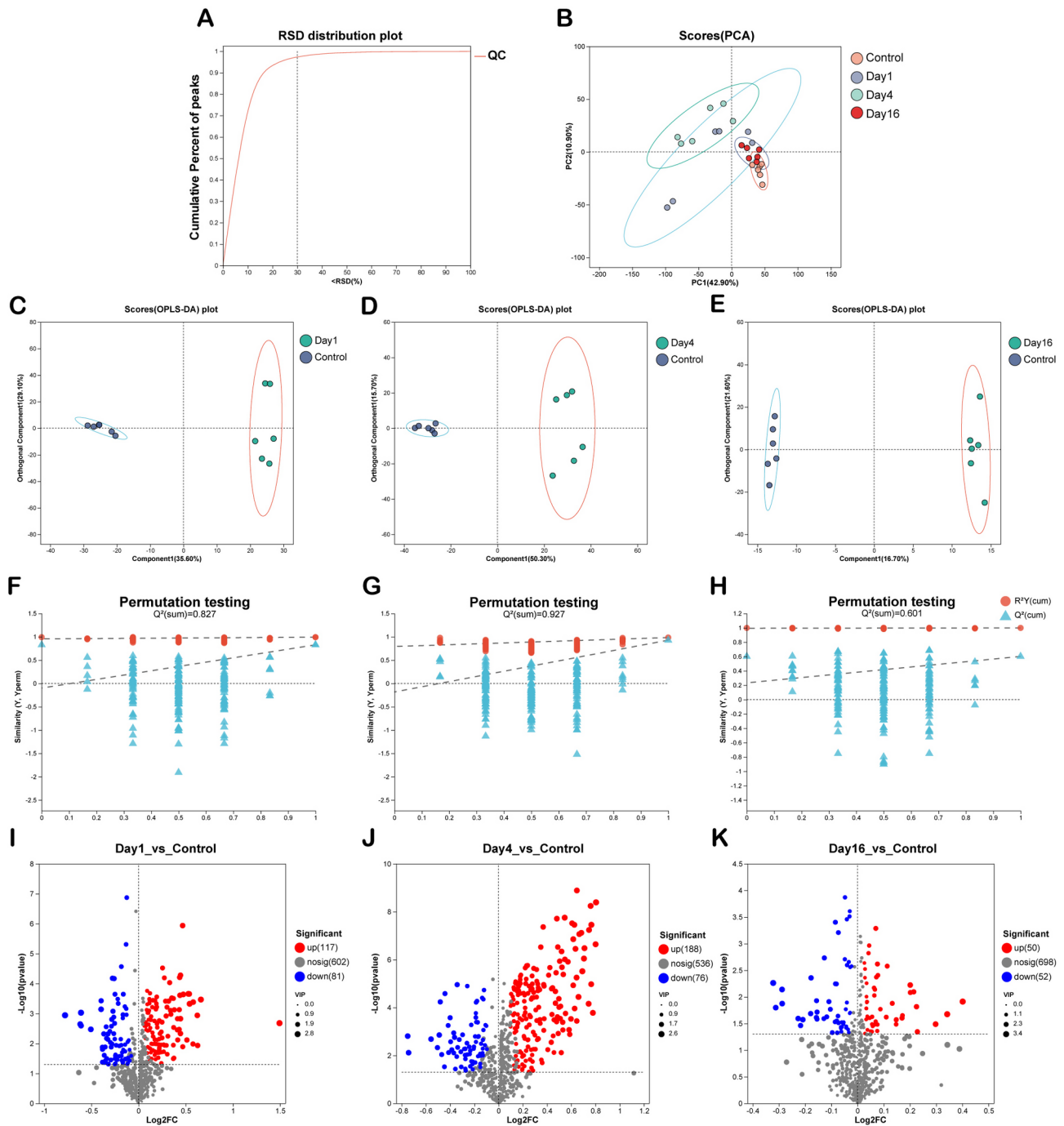


Fig. 2 Changes in the metabolic spectrum of skeletal muscle during the process of skeletal muscle regeneration. **(A)** QC sample assessment chart. **(B)** PCA of 3 stages of skeletal muscle regeneration (Day 1, Day 4, Day 16 after CTX injection) and the control group. **(C-E)** OPLS-DA plots of metabolites in skeletal muscle between the process of skeletal muscle regeneration and the control group (**(C)** inflammatory response stage, **(D)** repair stage, **(E)** remodeling stage). **(F-H)** Permutation test charts of OPLS-DA of metabolites in skeletal muscle during the process of skeletal muscle regeneration (**(F)** inflammatory response stage, **(G)** repair stage, **(H)** remodeling stage). **(I-K)** Volcano plots of differences in skeletal muscle metabolites between the process of skeletal muscle regeneration and the control group, with red representing upregulated metabolites and blue representing downregulated metabolites (**(I)** inflammatory response stage, **(J)** repair stage, **(K)** remodeling stage)

testing. PCA and OPLS-DA score plots showed significant separation among different stages of skeletal muscle regeneration and the control group (Figs. 2B-E). For OPLS-DA analysis, Q^2 in the OPLS-DA permutation test plot represents the predictive ability of the model. Generally, $Q^2 > 0.5$ indicates a good predictive ability of the model and no overfitting. In this study, the Q^2 of the OPLS-DA model for skeletal muscle samples was all > 0.5 (Figs. 2F-H). According to the OPLS-DA model ($VIP > 1$) and independent sample t-test ($p < 0.05$), compared with the control group, a total of 414 DEMs were screened out during the process of skeletal muscle regeneration. The results of DEMs are presented as a volcano plot. During the inflammatory response stage, 198 DEMs were screened out (117 upregulated and 81 downregulated)

(Fig. 2I). During the muscle repair stage, 264 DEMs were screened out (188 upregulated and 76 downregulated) (Fig. 2J). During the remodeling stage, 102 DEMs were screened out (50 upregulated and 52 downregulated) (Fig. 2K).

Screening and identification of DEMs in skeletal muscle tissues

Next, hierarchical clustering analysis was performed on the top 100 differentially abundant metabolites to reveal the expression patterns during different stages of skeletal muscle regeneration, depicted in a heatmap (Fig. 3). Subsequently, the differentially expressed metabolites from the 3 stages of skeletal muscle regeneration were classified according to HMDB compound categories. It was

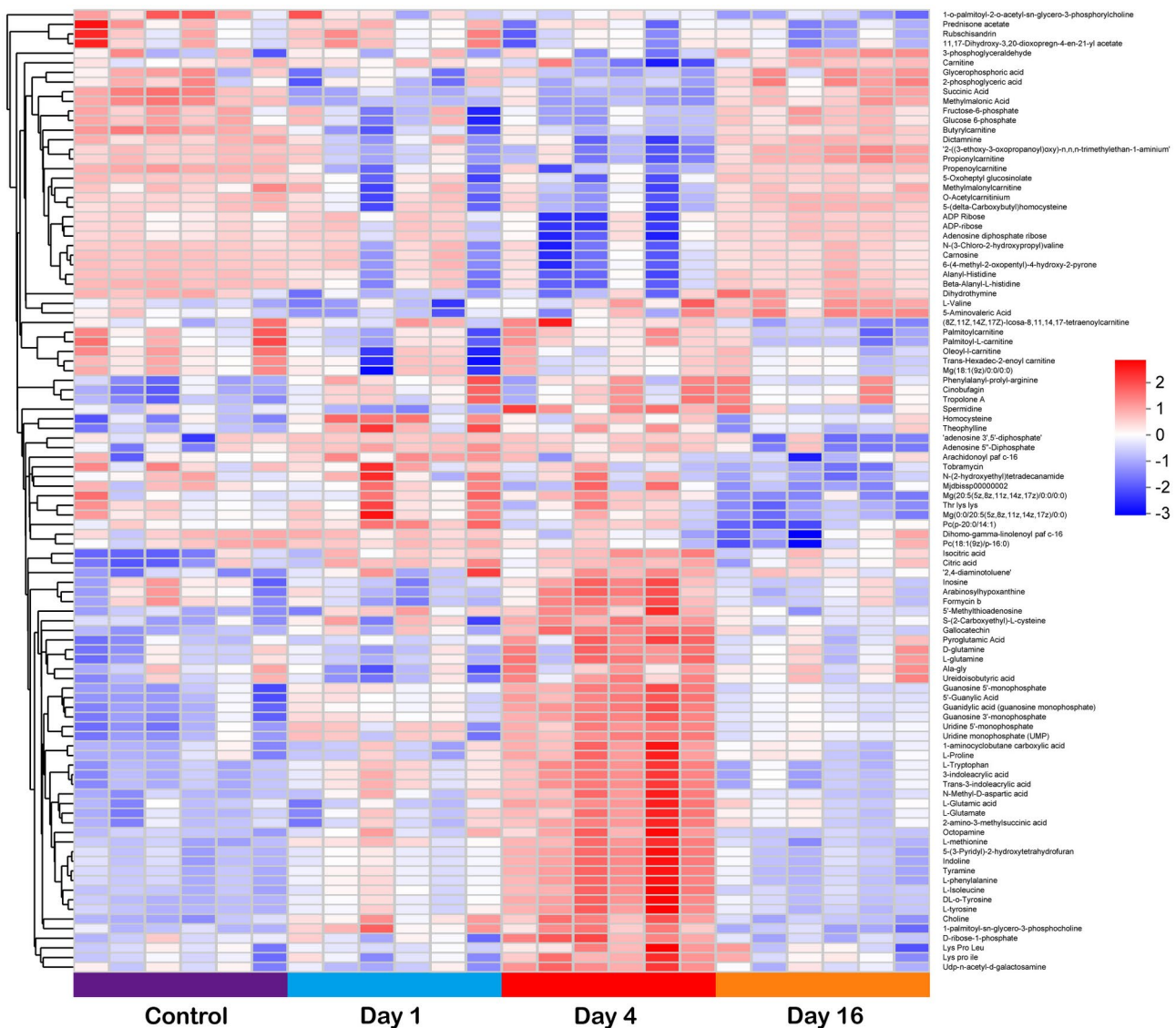


Fig. 3 Hierarchical clustering analysis of differential skeletal muscle metabolites in various stages of skeletal muscle regeneration. Colors such as purple, blue, red, and orange represent the control group, inflammatory response stage, repair stage, and remodeling stage, respectively

found that in the inflammatory response stage, the DEMs in skeletal muscle mainly belonged to Organic acid and derivatives (35.22%) and Lipids and lipid-like molecules (19.50%) (Fig. 4A). In the repair stage, the DEMs in skeletal muscle were mainly annotated in Organic acid and derivatives (35.91%), Nucleosides, nucleotides, and analogues (13.64%), Lipids and lipid-like molecules (12.73%), Organic oxygen compounds (12.27%), and Organoheterocyclic compounds (11.82%) (Fig. 4B). In the remodeling stage, the DEMs in skeletal muscle mainly belonged to Lipids and lipid-like molecules (29.56%), Organic acid and derivatives (26.76%), and Nucleosides, nucleotides, and analogues (18.31%) (Fig. 4C).

Metabolic pathway analysis in skeletal muscle tissues

Next, we performed KEGG pathway enrichment analysis on the DEMs identified during the process of skeletal muscle regeneration. We found that during the inflammatory response stage, the skeletal muscle metabolites were mainly involved in pathways such as the Calcium signaling pathway, Arginine biosynthesis, Antifolate resistance, Choline metabolism, and Glycerophospholipid metabolism (Fig. 5A, $p < 0.05$). During the repair stage, DEMs were primarily associated with pathways like the AMPK signaling pathway, FoxO signaling pathway, Arginine and proline metabolism, mTOR signaling pathway, D-Amino acid metabolism, Glutathione metabolism, Aminoacyl-tRNA biosynthesis, and Protein digestion and absorption (Fig. 5B, $p < 0.05$). During the remodeling stage, DEMs were predominantly involved in pathways including the FoxO signaling pathway, Alanine, aspartate and glutamate metabolism, and Galactose metabolism (Fig. 5C, $p < 0.05$).

Screening and analysis of common differential skeletal muscle metabolites

From the Venn diagram, it can be observed that among all the differential skeletal muscle metabolites in the process of skeletal muscle regeneration, 28 metabolites are common, 39 are unique to the inflammatory response stage, 35 are unique to the repair stage, and 104 are unique to the remodeling stage (Fig. 6A). Next, a temporal analysis was conducted on these 28 common DEMs to observe their expression patterns across the 3 stages of skeletal muscle regeneration. Using the Short Time-series Expression Miner (STEM) clustering algorithm and independent sample t-test ($p < 0.05$), two profiles were selected, namely profile1 and profile8 (Fig. 6B). Interestingly, the temporal trends of metabolites in profile1 and profile8 show an initial change (increase or decrease) followed by recovery, which aligns with the process of skeletal muscle regeneration (Figs. 6C-D). Profile1 includes 6 metabolites: 1-[(2R,5R)-4-Azidoxy-5-(hydroxymethyl)oxolan-2-yl]-5-methylpyrimidine-2,4-dione,

3-Hydroxyhexanoylcarnitine, L-Hexanoylcarnitine, Hexanoyl-L-carnitine, 7,8-dihydroneopterin 3'-phosphate, and (R)-Lipoic acid. In profile8, there are 5 metabolites: Diethylpropion, N-acetylaspartylglutamic acid, Undecylenic acid, 4-Oxo-L-proline, and Imidazoleacetic acid riboside. Subsequently, hierarchical clustering analysis based on the relative abundance of these 28 metabolites reveals that their changing trends broadly coincide with the process of skeletal muscle remodeling following CTX-induced muscle dissolution (Fig. 6E). Furthermore, KEGG functional enrichment analysis was performed on these metabolites, and pathways were ranked based on increasing p-values. The main enrichment was observed in the AMPK signaling pathway, Insulin resistance, and Antifolate resistance (Fig. 6F, $p < 0.05$).

Discussion

Past studies have shown that in-depth research into skeletal muscle metabolites can reveal key metabolic processes and molecules that affect muscle regeneration [16]. A thorough understanding of the impact of skeletal muscle metabolites on the skeletal muscle regeneration process aids in the discovery of key metabolites, providing direction for the treatment of skeletal muscle injuries and promoting their regeneration [17, 18]. However, the vast majority of skeletal muscle metabolomics studies are focused on mice, with relatively few studies conducted on large mammals [19]. Therefore, we chose pigs as the experimental animals, constructed a skeletal muscle regeneration model by injecting CTX, and conducted in-depth analysis of the metabolic characteristics during the 3 stages of the skeletal muscle regeneration process [20]. The aim is to systematically explore the dynamic process of mechanistic changes during pig skeletal muscle regeneration, in order to delve into the cellular mechanisms involved in the process of muscle regeneration.

The research results of Kumar et al. indicate that during MuSCs proliferation and differentiation, there are global changes in skeletal muscle metabolites, with significant metabolic profile characteristics at different stages [21]. We identified all metabolites at the 3 stages of skeletal muscle regeneration and found that the metabolic profile undergoes significant changes as skeletal muscle transitions from the inflammatory, repair to remodeling stages. Subsequently, through KEGG enrichment analysis of the DEMs at the 3 stages, we found that Cyclic ADP ribose is significantly downregulated during the inflammatory stage of skeletal muscle regeneration. Cyclic ADP ribose is a messenger of calcium signaling, and Berridge has pointed out that the calcium signaling pathway can regulate the transcription and secretion of inflammatory factors, with changes in intracellular calcium signaling potentially affecting the extent and duration of inflammatory responses [22]. Therefore, we

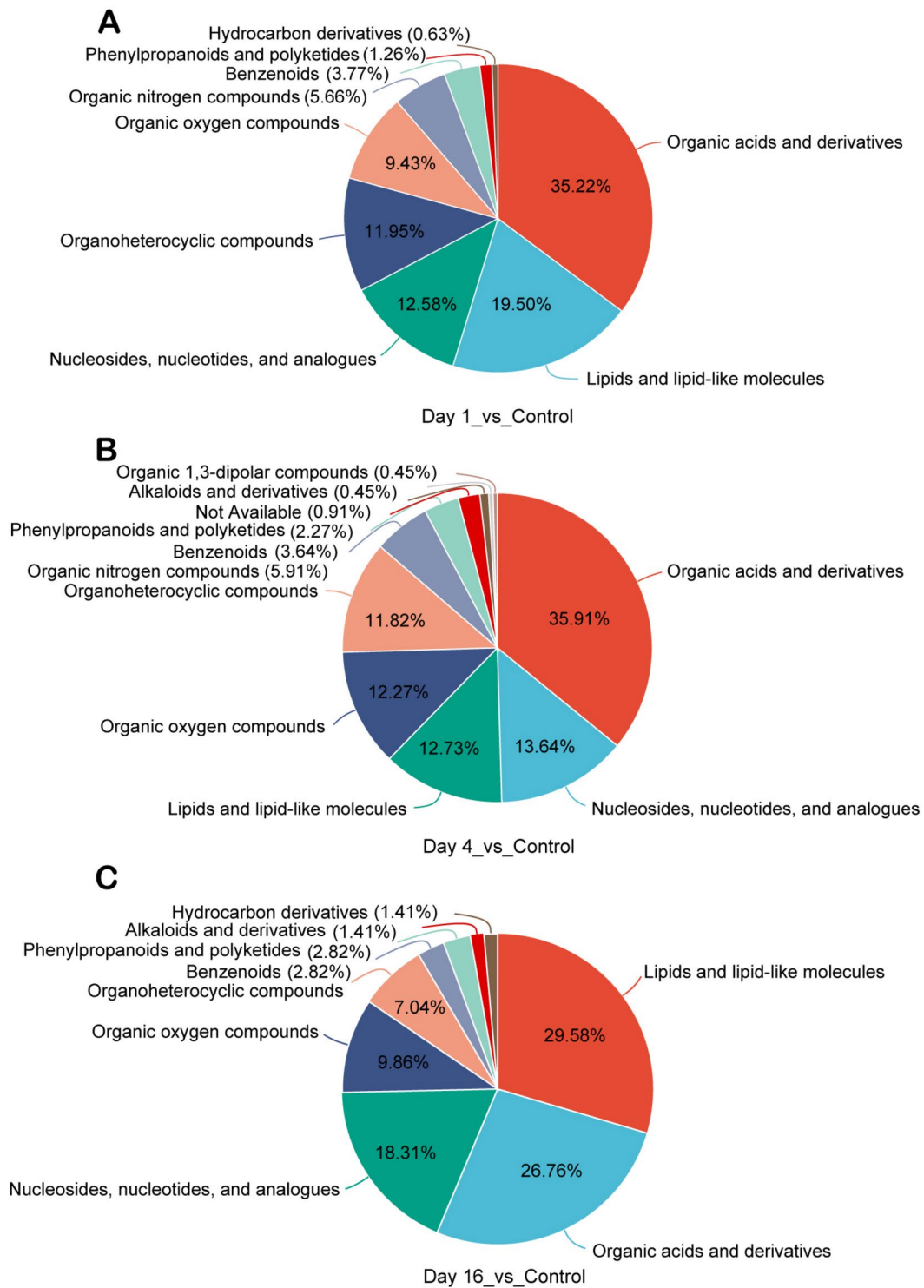


Fig. 4 Classification of differential skeletal muscle metabolites during skeletal muscle regeneration. **(A-C)** Pie charts of HMDB compound classification of DEMs in skeletal muscle comparing the 3 stages of skeletal muscle regeneration with the control group (**(A)** inflammatory response stage, **(B)** repair stage, **(C)** remodeling stage)

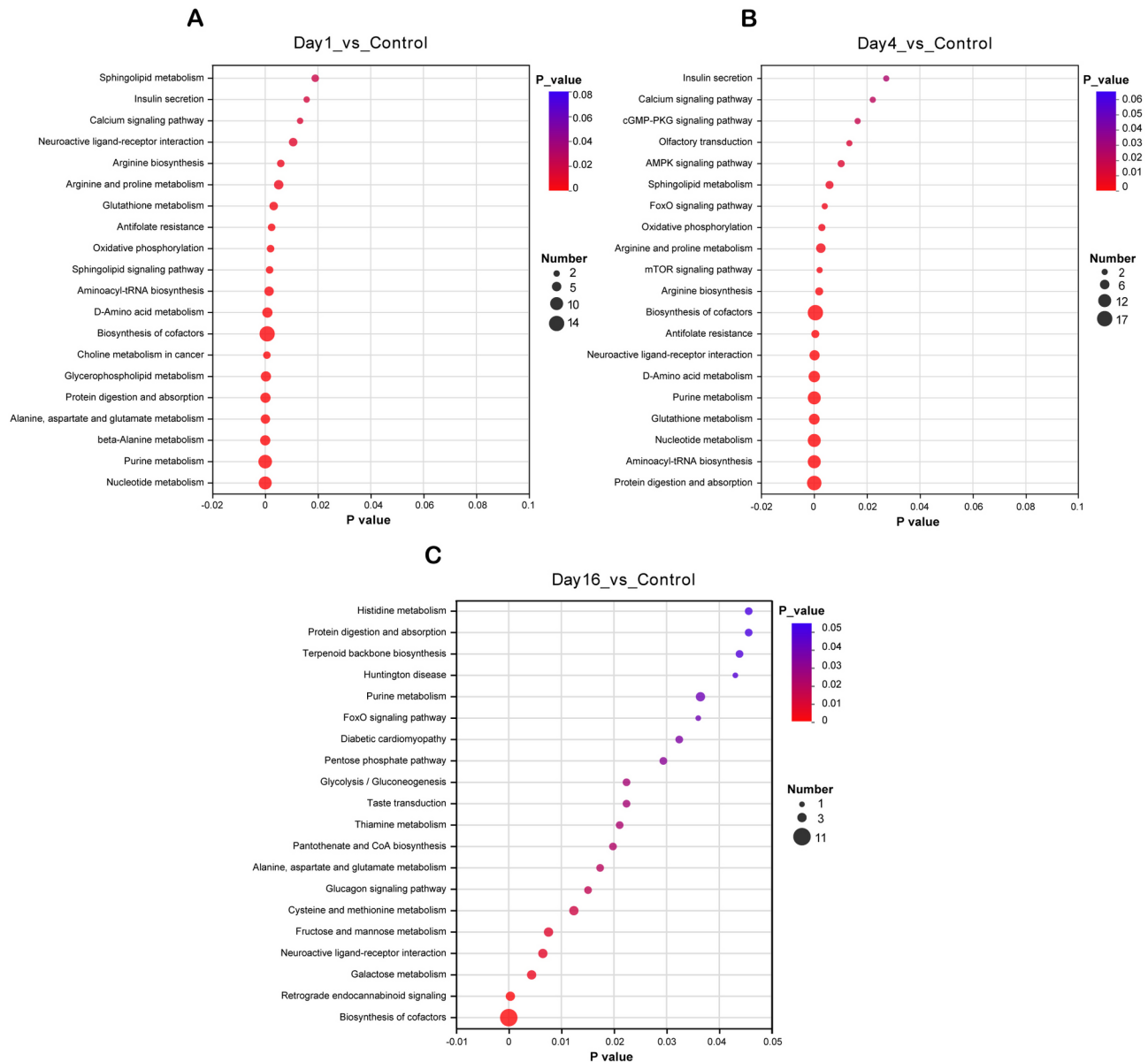


Fig. 5 Functional analysis of skeletal muscle DEMs in the 3 stages of skeletal muscle regeneration. (A-C) KEGG pathway enrichment analysis of differential skeletal muscle metabolites comparing each stage of skeletal muscle regeneration with the control group ((A) inflammatory response stage, (B) repair stage, (C) remodeling stage)

speculate that after injecting CTX, the calcium signaling pathway may be inhibited, thereby regulating the secretion of related inflammatory factors to alleviate the inflammatory response, although this hypothesis requires further validation. At the same stage, the content of L-Arginine in metabolites is significantly upregulated. In mammals, arginine methylation is catalyzed by the protein arginine methyltransferase (PRMT) family [23]. Arginine methylation coordinates skeletal muscle repair and regeneration through various mechanisms, including activating MuSCs, regulating transcription factors, influencing intracellular signaling pathways,

modulating inflammatory responses, and promoting the action of growth factors [24–26]. Therefore, it can be inferred that during the inflammatory stage, skeletal muscle cells may upregulate the arginine biosynthesis pathway, resulting in increased L-arginine content. This increase may subsequently enhance arginine methylation, regulate inflammatory responses, and promote skeletal muscle repair. Seong et al.’s research indicates that folate is a precursor to various coenzymes and is crucial for normal skeletal muscle cell development. Folate deficiency not only inhibits proliferation but also leads to a significant increase in DNA damage in skeletal muscle

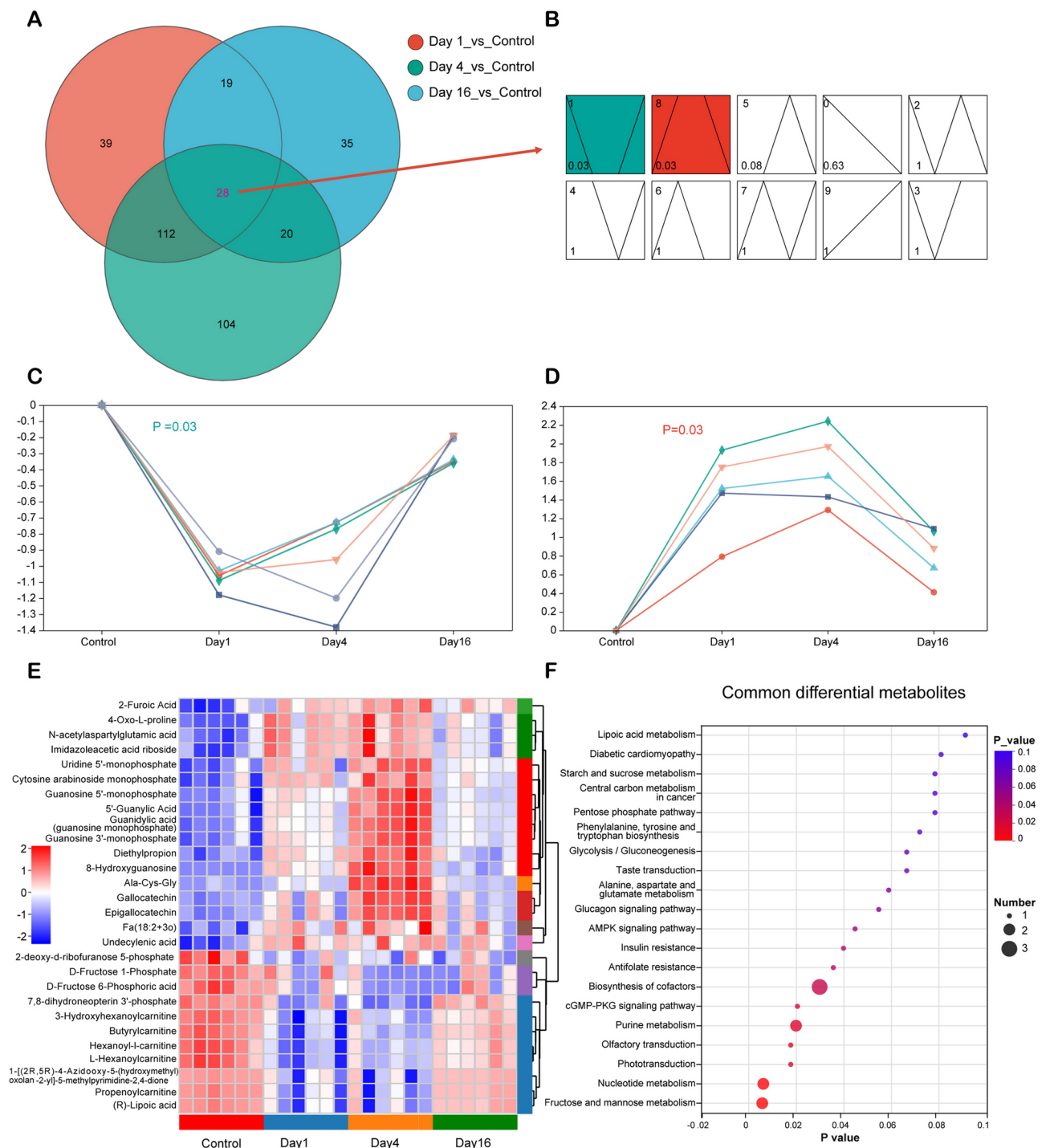


Fig. 6 Analysis of common differential skeletal muscle metabolites during the process of skeletal muscle regeneration. **(A)** Venn diagram of differential skeletal muscle metabolites comparing the 3 stages of skeletal muscle regeneration with the control group, **(B-D)** Temporal expression analysis of the 28 common differential skeletal muscle metabolites (**B**) Temporal expression analysis, **(C)** Profile1 trend graph, **(D)** Profile8 trend graph), **(E)** Hierarchical clustering analysis of the 28 common differential skeletal muscle metabolites. Colors such as red, blue, yellow, and green represent the control group, inflammatory response stage, repair stage, and remodeling stage, respectively. **(F)** KEGG pathway enrichment analysis of common DEMs

cells [27, 28]. In our study, the content of folate was significantly increased, suggesting that skeletal muscle cells may release folate to alleviate DNA damage. Research by Li and colleagues has shown that CTX can hydrolyze phospholipids in the cell membrane through its phospholipase activity, damaging the integrity of the cell membrane [29]. Phospholipids consist of glycerol, fatty acids, and phosphate groups, with phosphatidylcholine (PC) and choline being important components of the phosphate groups. This mechanism may explain the significant increase in PC and choline levels we observed, which in turn affects the choline metabolism pathway.

During the skeletal muscle repair phase, the muscle fibers at the site of injury have completely dissolved, while MuSCs repair the damage through proliferation and differentiation. Adenosine monophosphate-activated protein kinase (AMPK) is a protein kinase activated by Adenosine monophosphate (AMP), and both excessive activation and deficiency of AMPK can affect skeletal muscle regeneration [30]. In our study, the content of AMP is significantly upregulated during the skeletal muscle repair phase. Therefore, we speculate that the upregulated AMP content may appropriately modulate the expression of AMPK, thereby influencing skeletal muscle repair. During the repair phase, our data show that the expression levels of glutamate and arginine metabolic products are also significantly upregulated. Supplementing with glutamate has been found to regulate the FoxO and mTOR pathways to alleviate muscle protein loss [31]. At the same time, the increase in arginine can activate the mTOR signaling pathway to promote muscle protein synthesis [32, 33]. These findings support our hypothesis: In skeletal muscle, it may promote regeneration by upregulating metabolite levels such as glutamate and arginine, and regulating key metabolic pathways such as FoxO signaling pathway, mTOR signaling pathway, Arginine and proline metabolism, Aminoacyl-tRNA biosynthesis. In addition, during skeletal muscle remodeling phase, we also observed a significant upregulation of L-glutamate and L-valine levels. Previous research has confirmed that FoxO plays a key role in regulating protein synthesis and muscle atrophy [34]. L-glutamate may regulate the FoxO signaling pathway and alleviate muscle protein loss by inhibiting the mRNA expression of TLR4 and NODs signaling-related genes [31]. D-galactose induces muscle fibrosis, and excessive fibrosis impairs muscle regeneration [35]. Our data show that the metabolism of UDP-D-Galactose is significantly downregulated. Therefore, we speculate that during the skeletal muscle remodeling phase, skeletal muscles upregulate the metabolism of L-glutamate, L-valine, and others, while downregulating the metabolism of UDP-D-Galactose and others. This regulates pathways such as the FoxO signaling pathway, Alanine, aspartate and glutamate metabolism,

and Galactose metabolism, inhibiting the loss of skeletal muscle protein, promoting the deposition of skeletal muscle protein, and accelerating skeletal muscle regeneration. In summary, the 3 stages of the skeletal muscle regeneration process are significantly different but interconnected. These results clarify the connection between metabolomic changes and the mechanisms of skeletal muscle regeneration, providing important information for regulating skeletal muscle regeneration in pigs and offering guidance for research on regulating human skeletal muscle regeneration.

To understand the metabolites associated with skeletal muscle regeneration and to further investigate their potential role in the regeneration process, we analyzed the temporal expression of 28 common differential DEMs in 3 stages. We found that all of these metabolites showed either an upward and then downward trend or a downward and then upward trend, related to the mechanisms involved in the regeneration process of these metabolites in skeletal muscle. Our study showed that (R)-Lipoic acid metabolism was first down-regulated and then increased. (R)-Lipoic acid is a chiral form of α -Lipoic acid (α -LA). Previous studies have found that α -Lipoic acid, as an inducer of hydrogen peroxide (H_2O_2) and nitric oxide (NO) and a regulator of the thiol redox state, its intake may help improve skeletal muscle regeneration. This process is mainly achieved by altering the inflammatory response related to the production of H_2O_2 and NO and the thiol redox state [36]. We speculate that during the inflammation and repair phases, (R)-Lipoic acid may be excessively consumed due to its inhibitory effect on the inflammatory response, resulting in a significant reduction in its total amount in the muscles. In the subsequent remodeling phase, as the inflammation subsides, (R)-Lipoic acid gradually returns to normal levels. Therefore, the total amount of (R)-Lipoic acid shows a trend of first decreasing and then increasing, but further research is required to confirm this. 8-Hydroxyguanosine and Uridine 5'-monophosphate (5'-UMP) both showed a trend of increasing and then decreasing. Past studies have shown that 8-Hydroxyguanosine is a DNA damage marker [37, 38]. We believe that during the skeletal muscle regeneration process following CTX injection, DNA damage occurs and is subsequently repaired. 8-Hydroxyguanosine may serve as a potential biomarker for skeletal muscle regeneration after injury, providing new targets for promoting skeletal muscle regeneration. Kosuke et al. showed that 5'-UMP promotes myogenic differentiation and mitochondrial biogenesis and increases slow muscle fibers through activation of MYOG and PGC-1 α to promote muscle growth and alleviate muscle atrophy [39, 40]. This is the same as our result that 5'-UMP expression was highest during the repair phase, so we hypothesize that mainly during the repair phase, skeletal muscle

cells are regulated to increase 5'-UMP metabolism and promote the regeneration of skeletal muscle cells, and this conjecture needs to be further verified. The metabolism of the above 3 DEMs is fundamentally consistent with the process of skeletal muscle regeneration, and all play a significant role in the metabolic process. We believe that (R)-Lipoic acid, 8-Hydroxyguanosine, and 5'-UMP may be key metabolites in the metabolic mechanism of skeletal muscle regeneration. Through in-depth research on these metabolites, we can better understand the molecular mechanisms of skeletal muscle regeneration, providing new insights for the treatment of skeletal muscle injuries. Next, KEGG pathway analysis was performed on these 28 DEMs, revealing genes involved in AMPK signaling pathway, Insulin resistance. In skeletal muscle, gluconeogenesis can be inhibited by inhibiting 1,6-bisphosphate fructose kinase as well as insulin inhibitory factor [41, 42]. This is consistent with our findings, and we hypothesize that down-regulation of D-Fructose 6-Phosphoric acid metabolism through D-Fructose 6-Phosphoric acid metabolism may affect gluconeogenesis, which modulates skeletal muscle glucose uptake and influences energy acquisition during skeletal muscle regeneration. However, these hypotheses still need to be verified by subsequent experiments. In conclusion, our results further elucidate the influence of the skeletal muscle regeneration process on the composition of skeletal muscle metabolites, and also indicate that skeletal muscle metabolites can be involved in regulating the skeletal muscle regeneration process. These findings provide important clues for further research into the relationship between skeletal muscle regeneration and metabolism, and may be significant for promoting muscle repair and functional recovery.

However, our study has some limitations, as it only performed metabolomic analysis of the skeletal muscle regeneration process. Although it revealed the metabolic mechanisms of skeletal muscle regeneration, further analysis using multi-omics techniques and related experimental validation is needed. Additionally, we did not consider the differences in regeneration mechanisms among different muscle fiber types in our study, which will be addressed in future research to distinguish the varying roles of different muscle fiber types in the regeneration process. We identified a number of skeletal muscle metabolites that may become key metabolites for skeletal muscle regeneration. Based on these results, future studies need to further verify the molecular mechanisms of potential key metabolites in skeletal muscle and explore the gene interactions during skeletal muscle regeneration, which will provide a basis for developing new muscle regeneration treatment strategies.

Conclusions

The aim of this study was to investigate the metabolic differences and important signaling pathways involved in the process of skeletal muscle regeneration using pigs as a model. Metabolomics technology was utilized to reveal the mechanisms of skeletal muscle regeneration, and the analysis of the time series of common DEMs identified some key metabolites that reflect the degree of skeletal muscle regeneration. These results provide theoretical references for regulating skeletal muscle regeneration.

Abbreviations

LC	Liquid chromatography
MS	Mass spectrometry
CTX	Cardiotoxin
DEMs	Differential expressed metabolites
FGF	Fibroblast growth factor
11,12-EET	11,12-epoxyeicosatrienoic acid
α -KG	α -ketoglutarate
AMP	Adenosine monophosphate
AMPK	Adenosine monophosphate-activated protein kinase
PVDF	Polyvinylidene fluoride.
FoxO	Forkhead box O
mTOR	mammalian target of rapamycin
LDH	Lactate dehydrogenase
HMDB	Human Metabolome Database
MYH3	Myosin Heavy Chain 3
RSD	Relative standard deviation
OPLS-DA	Orthogonal partial least squares discriminant analysis
PCA	Principal component analysis
VIP	Variable importance in projection
QC	Quality control
KEGG	Kyoto Encyclopedia of Genes and Genomes
STEM	Short Time-series Expression Miner
H&E	Hematoxylin-Eosin staining
PCNA	Proliferating Cell Nuclear Antigen
Pax7	Paired Box 7
MuSCs	Muscle satellite cells
PRMT	Protein arginine methyltransferase
PC	Phosphatidylcholine
5'-UMP	Uridine 5'-monophosphate
α -LA	α -Lipoic acid

Supplementary Information

The online version contains supplementary material available at <https://doi.org/10.1186/s12891-025-08703-y>.

Supplementary Material 1

Supplementary Material 2

Acknowledgements

Not applicable.

Author contributions

Conceptualization, H.M.; data curation, L.Y., K.W.; formal analysis, S.L.F., B.C. and X.L.; investigation, W.C., C.L., J.L. and X.X.; methodology, Y.L.; writing—original draft, Y.L.; writing—review and editing: H.M. All authors have read and agreed to the published version of the manuscript.

Funding

This work was supported by Biological Breeding-National Science and Technology Major Project (No.2023ZD04046), Research and Application of Key Technologies for High-Efficiency Breeding of Tibetan Pigs (XZ202501ZY0143), Research and Application of Superior Germplasm Resources and Key Technologies for Efficient Breeding of Tibetan Pigs (SNQYKJXT-01), Major Science and Technology Special Plan of Yunnan Province (202202AE090032),

The program of talent of science & technology and platforms of Yunnan Province (202305AF150211), Postgraduate Scientific Research Innovation Project of Hunan Province (CX20230713), Postgraduate Scientific Research Innovation Project of Hunan Agriculture University (2023XC006), and the Hunan Provincial Department of Education Scientific Research Project (23B1097).

Data availability

Data is provided within the manuscript or supplementary information files.

Declarations

Ethics approval and consent to participate

All animal experiments in this study were approved by the Institutional Animal Care and Use Committee of Hunan Agricultural University, Changsha, Hunan Province, China, with approval number CACAHU 20230701. Written informed consent was obtained before sample collection from the commercial farm.

Competing interests

The authors declare no competing interests.

Author details

¹College of Animal Science and Technology, Hunan Agricultural University, Changsha, PR 410128, China

²Key Laboratory of Livestock and Poultry Resources (Pig) Evaluation and Utilization, Ministry of Agriculture and Rural Affairs, Changsha, PR 410128, China

³Yuelushan Laboratory, Changsha, PR 410128, China

Received: 27 November 2024 / Accepted: 25 April 2025

Published online: 09 May 2025

References

1. Song H, Tian X, He L, Liu D, Li J, Mei Z, et al. CREG1 deficiency impaired myoblast differentiation and skeletal muscle regeneration. *J Cachexia Sarcopenia Muscle*. 2024;15:587–602.
2. De Micheli AJ, Laurillard EJ, Heinke CL, Ravichandran H, Fraczek P, Soueid-Baumgarten S, et al. Single-cell analysis of the muscle stem cell hierarchy identifies heterotypic communication signals involved in skeletal muscle regeneration. *Cell Rep*. 2020;30:3583–e35955.
3. Wosczyzna MN, Rando TA. A muscle stem cell support group: coordinated cellular responses in muscle regeneration. *Dev Cell*. 2018;46:135–43.
4. Shang M, Cappellesso F, Amorim R, Serneels J, Virga F, Eelen G, et al. Macrophage-derived glutamine boosts satellite cells and muscle regeneration. *Nature*. 2020;587:626–31.
5. Nunez-Alvarez Y, Hurtado E, Munoz M, Garcia-Tunon I, Rech GE, Pluvinet R et al. Loss of HDAC11 accelerates skeletal muscle regeneration in mice. *FEBS J*. 2020;23.
6. Ance S, Stuellsatz P, Feige JN. Muscle stem cell quiescence: controlling stemness by staying asleep. *Trends Cell Biol*. 2021;31:556–68.
7. Chi Z, Chen S, Yang D, Cui W, Lu Y, Wang Z, et al. Gasdermin D-mediated metabolic crosstalk promotes tissue repair. *Nature*. 2024;634:1168–77.
8. Ciuffoli V, Feng X, Jiang K, Acevedo-Luna N, Ko KD, Wang AHJ, et al. Psat1-generated α -ketoglutarate and glutamine promote muscle stem cell activation and regeneration. *Genes Dev*. 2024;38:151–67.
9. Graca FA, Stephan A, Minden-Birkenmaier BA, Shirinifard A, Wang Y-D, Demontis F, et al. Platelet-derived chemokines promote skeletal muscle regeneration by guiding neutrophil recruitment to injured muscles. *Nat Commun*. 2023;14:2900.
10. Alseekh S, Aharoni A, Brotman Y, Contrepois K, D'Auria J, Ewald J, et al. Mass spectrometry-based metabolomics: a guide for annotation, quantification and best reporting practices. *Nat Methods*. 2021;18:747–56.
11. Lunney JK, Van Goor A, Walker KE, Hailstock T, Franklin J, Dai C. Importance of the pig as a human biomedical model. *Sci Transl Med*. 2021;13:eabd5758.
12. Wang L, Jia Z, Xu K, Zhang F, Yin Y. When will dual-purpose pigs fly? *Innov*. 2024;5:100702.
13. Garry GA, Antony ML, Garry DJ. Cardiotoxin induced injury and skeletal muscle regeneration. In: Kyba M, editor. *Skeletal muscle regeneration in the mouse*. New York, NY: Springer New York; 2016. pp. 61–71.
14. Ma J, Zhu Y, Zhou X, Zhang J, Sun J, Li Z, et al. miR-205 regulates the fusion of Porcine myoblast by targeting the myomaker gene. *Cells*. 2023;12:1107.
15. Wang Y, Lu J, Liu Y. Skeletal muscle regeneration in Cardiotoxin-Induced muscle injury models. *Int J Mol Sci*. 2022;23:13380.
16. Maroto R, Graber TG, Romsdahl TB, Kudlicki A, Russell WK, Rasmussen BB. Metabolomic and lipidomic signature of skeletal muscle with constitutively active mechanistic target of Rapamycin complex 1. *J Nutr*. 2023;153:3397–405.
17. Rimmer LA, Geisbrecht ER, Chao MD, O'Quinn TG, Woodworth JC, Zumbaugh MD. Skeletal muscle metabolism is dynamic during Porcine postnatal growth. *Metabolites*. 2024;14:357.
18. Cervenka I, Agudelo LZ, Ruas JL. Kynurenines: Tryptophan's metabolites in exercise, inflammation, and mental health. *Science*. 2017;357:eaaf9794.
19. Uchitomi R, Hatazawa Y, Senoo N, Yoshioka K, Fujita M, Shimizu T, et al. Metabolomic analysis of skeletal muscle in aged mice. *Sci Rep*. 2019;9:10425.
20. Guardiola O, Andolfi G, Tirone M, Iavarone F, Brunelli S, Minchiotti G. Induction of acute skeletal muscle regeneration by cardiotoxin injection. *J Vis Exp*. 2017;:54515.
21. Kumar A, Kumar Y, Sevak JK, Kumar S, Kumar N, Gopinath SD. Metabolomic analysis of primary human skeletal muscle cells during myogenic progression. *Sci Rep*. 2020;10:11824.
22. Berridge MJ. The inositol trisphosphate/calcium signaling pathway in health and disease. *Physiol Rev*. 2016;96:1261–96.
23. Li W, He Y, Yang J, Hu G, Lin Y, Ran T, et al. Profiling PRMT methylome reveals roles of hnRNPA1 arginine methylation in RNA splicing and cell growth. *Nat Commun*. 2021;12:1946.
24. Blanc RS, Richard S. Regenerating muscle with arginine methylation. *Transcription*. 2017;8:175–8.
25. Ma D, Yang M, Wang Q, Sun C, Shi H, Jing W, et al. Arginine methyltransferase PRMT5 negatively regulates cGAS-mediated antiviral immune response. *Sci Adv*. 2021;7:eabc1834.
26. Blanc RS, Vogel G, Chen T, Crist C, Richard S. PRMT7 preserves satellite cell regenerative capacity. *Cell Rep*. 2016;14:1528–39.
27. Hwang SY, Kang YJ, Sung B, Jang JY, Hwang NL, Oh HJ, et al. Folic acid is necessary for proliferation and differentiation of C2C12 myoblasts. *J Cell Physiol*. 2018;233:736–47.
28. Hwang SY, Sung B, Kim ND. Roles of folate in skeletal muscle cell development and functions. *Arch Pharm Res*. 2019;42:319–25.
29. Li F, Shrivastava IH, Hanlon P, Dagda RK, Gasanoff ES. Molecular mechanism by which Cobra venom cardiotoxins interact with the outer mitochondrial membrane. *Toxins*. 2020;12:425.
30. Thomson DM. The role of AMPK in the regulation of skeletal muscle size, hypertrophy, and regeneration. *Int J Mol Sci*. 2018;19:3125.
31. Guo A, Li K, Tian H, Fan Z, Chen Q, Yang Y, et al. FGF19 protects skeletal muscle against obesity-induced muscle atrophy, metabolic derangement and abnormal Irisin levels via the AMPK/SIRT-1/PGC- α pathway. *J Cell Mol Med*. 2021;25:3585–600.
32. Yao K, Yin Y-L, Chu W, Liu Z, Deng D, Li T, et al. Dietary arginine supplementation increases mTOR signaling activity in skeletal muscle of neonatal pigs. *J Nutr*. 2008;138:867–72.
33. Zhou M, Wei Y, Feng Y, Zhang S, Ma N, Wang K, et al. Arginine regulates skeletal muscle fiber type formation via mTOR signaling pathway. *Int J Mol Sci*. 2024;25:6184.
34. Chen K, Gao P, Li Z, Dai A, Yang M, Chen S, et al. Forkhead box O signaling pathway in skeletal muscle atrophy. *Am J Pathol*. 2022;192:1648–57.
35. Wu Y, Wu Y, Yang Y, Yu J, Wu J, Liao Z, et al. Lysyl oxidase-like 2 inhibitor rescues D-galactose-induced skeletal muscle fibrosis. *Aging Cell*. 2022;21:e13659.
36. Zembron-Lacny A, Gajewski M, Naczek M, Dziewiecka H, Siatkowski I. Physical activity and alpha-lipoic acid modulate inflammatory response through changes in thiol redox status. *J Physiol Biochem*. 2013;69:397–404.
37. Abe T, Isobe C, Murata T, Sato C, Tohgi H. Alteration of 8-hydroxyguanosine concentrations in the cerebrospinal fluid and serum from patients with Parkinson's disease. *Neurosci Lett*. 2003;336:105–8.
38. Guo C, Chen Q, Chen J, Yu J, Hu Y, Zhang S, et al. 8-Hydroxyguanosine as a possible RNA oxidative modification marker in urine from colorectal cancer patients: evaluation by ultra performance liquid chromatography-tandem mass spectrometry. *J Chromatogr B*. 2020;1136:121931.
39. Nakagawara K, Takeuchi C, Ishige K. 5'-CMP and 5'-UMP promote myogenic differentiation and mitochondrial biogenesis by activating Myogenin and PGC-1 α in a mouse myoblast C2C12 cell line. *Biochem Biophys Res*. 2022;31:101309.

40. Nakagawara K, Takeuchi C, Ishige K. 5'-CMP and 5'-UMP alleviate dexamethasone-induced muscular atrophy in C2C12 myotubes. *Biochem Biophys Res Commun*. 2023;34:101460.
41. Vincent MF, Erion MD, Gruber HE, Van Den Berghe G. Hypoglycaemic effect of AICARiboside in mice. *Diabetologia*. 1996;39:1148–55.
42. Aschenbach WG, Hirshman MF, Fujii N, Sakamoto K, Howlett KF, Goodyear LJ. Effect of AICAR treatment on glycogen metabolism in skeletal muscle. *Diabetes*. 2002;51:567–73.

Publisher's note

Springer Nature remains neutral with regard to jurisdictional claims in published maps and institutional affiliations.